THE ASTROPHYSICAL JOURNAL, 529:1115–1130, 2000 February 1

PRECONDITIONING THE DIFFERENTIAL EMISSION MEASURE (T_e) INVERSE PROBLEM

S. W. MCINTOSH[1] AND P. CHARBONNEAU
High Altitude Observatory, National Center for Atmospheric Research,[2] P.O. Box 3000, Boulder, CO 80307-3000
AND
J. C. BROWN
Department of Physics and Astronomy, University of Glasgow, Glasgow, G12 8QQ, Scotland
Received 1999 May 4; accepted 1999 September 22

ABSTRACT

In an inverse problem of any kind, poor conditioning of the inverse operator decreases the numerical stability of any unregularized solution in the presence of data noise. In this paper we show that the numerical stability of the differential emission measure (DEM) inverse problem can be considerably improved by judicious choice of the integral operator. Specifically, we formulate a combinatorial optimization problem where, in a preconditioning step, a subset of spectral lines is selected in such a way as to minimize explicitly the condition number of the discretized integral operator. We tackle this large combinatorial optimization problem using a genetic algorithm. We apply this preconditioning technique to a synthetic data set comprising of solar UV/EUV emission lines in the *SOHO* SUMER/CDS wavelength range. Following which we test the same hypothesis on lines observed by the Harvard S-055 EUV spectroheliometer. On performing the inversion we see that the temperature distribution in the emitting region of the solar atmosphere is recovered with considerably better stability and smaller error bars when our preconditioning technique is used, in both synthetic and "real" cases, even though this involves the analysis of *fewer* spectral lines than in the "All-lines" approach. The preconditioning step leads to regularized inversions that compare favorably to inversions by singular value decomposition, while providing greater flexibility in the incorporation of physically and/or observationally based constraints in the line selection process.

Subject headings: methods: analytical — methods: numerical — Sun: atmosphere — Sun: UV radiation

1. INTRODUCTION

The launch of the *Solar and Heliospheric Observatory* (*SOHO*) in 1995 saw the largest complement of solar observing tools since the *Skylab* era. One of *SOHO*'s prime scientific goals is to understand the structure and dynamics of the Sun's chromospheric, transition region and coronal plasmas (Fleck, Domingo, & Poland 1995). This involves, in part, the study of the Sun's UV/EUV emission; this responsibility is principally undertaken by the Coronal Diagnostic Spectrometer (CDS; Harrison et al. 1995) and the Solar Ultraviolet Measurement of Emitted Radiation (SUMER; Wilhelm et al. 1995) instruments.

The characterization of the Sun's optically thin UV/EUV emission in terms of distributions of electron density, n_e, and electron temperature, T_e, depends on the determination of the emission measure functions, differential (DEM) or otherwise, of the atmosphere (Pottasch 1964; Withbroe 1970, 1975; Jordan & Wilson 1971; Munro, Dupree, & Withbroe 1971; Dere & Mason 1981; Raymond & Doyle 1981b; Doscheck 1987; Mason & Monsignori-Fossi 1994). These measures can, with additional physical assumptions, yield important information about the nature of the energy and momentum balance mechanisms of different components of the solar plasma. Only with reliable estimates, or diagnostics, can we possibly hope to carry out sound empirical investigations of the physical processes underlying coronal heating and/or solar wind acceleration.

Mathematically, the DEM(T_e) inverse problem takes the form of a Fredholm integral equation of the first kind, i.e.,

$$I_l = \int_{T_e} K_l(T_e)\xi(T_e)dT_e \text{ ergs cm}^{-2}\text{ sr}^{-1}\text{ s}^{-1}\,, \qquad (1)$$

where I_l is the line intensity of an emission line labeled l, $K_l(T_e)$ is the line emissivity, and $\xi(T_e)$ is the differential emission measure (DEM) in electron temperature. This quantity, the source function we seek to infer from the measured line intensities, is defined by Craig & Brown (1976) as

$$\xi(T_e) = \int_{S_{T_e}} \frac{n_e^2}{|\,T_e\,|}\, dS_{T_e} \text{ cm}^{-5}\text{ K}^{-1}\,, \qquad (2)$$

where S_{T_e} is a surface of constant T_e in the emitting volume of plasma and the integral over all such surfaces is its *general* form, describing the nonisothermal plasma. DEM(T_e) is basically a mean-square temperature gradient-weighted electron density but physically represents the distribution of n_e^2 through the various temperature regions along the line of sight. If the assumed/imposed atmospheric model is plane-parallel in nature, the complicated form of equation (2) reduces to the commonly used form of DEM [i.e., $\xi(T_e) = n_e^2\, dh/dT_e$ for scale height h; see discussion in Brown et al. 1991], although both, if treated correctly, should yield functions with the same characteristic shape.

The derivation of the above characteristic plasma distributions from remotely sensed data (i.e., essentially emission line intensities) represents an ill-posed inverse problem. The problem is ill-posed in the classical sense, in that *many* different DEMs can be inferred from the *same* observational data, i.e., there is a distinct nonuniqueness in *any* calculation (see, e.g., Craig & Brown 1976, 1986; Parker 1994, Chap. 2). In many ways this difficulty continues to pose a

[1] Also with the Advanced Study Program of the National Center for Atmospheric Research.
[2] The National Center for Atmospheric Research is sponsored by the National Science Foundation.

significant hurdle and has been discussed extensively in the recent literature (see, e.g., Thompson 1991; Judge et al. 1995; Kashyap & Drake 1998). However, if we adopt the view of Craig & Brown (1976) that the differential emission measure is the only meaningful quantity that can be inferred from frequency integrated UV/EUV line intensities, we must also address numerical problems associated with the numerical inverse problem, i.e., the numerical counterpart of ill-posedness known as poor conditioning.

In this paper we consider the problem of obtaining a small set of UV/EUV lines (predominantly belonging to the 150–1610 Å wavelength range of the CDS/SUMER instruments) such that the unavoidable poor conditioning of any numerical inversion is at least minimized. In order to achieve this optimizational goal we make use of a genetic algorithm to search through the possible subsets of lines to find those that lead to the least deleterious numerical conditioning of the discretized integral operator.

In § 2 we introduce the reader to some fundamental mathematical and physical tools, and provide an overview of the GA used in this analysis. An in-depth discussion of GA-related matters will be the subject of a future paper (McIntosh & Charbonneau 2000). We do provide a basic overview of the SELECTOR GA in § 2.5 and discuss in some detail some relevant run-time characteristics of a typical SELECTOR run.

In § 3, we show that when an optimal set lines are chosen by SELECTOR and are used to perform a DEM(T_e) inversion on some synthetic test data, the effect of any data errors propagating through to the solution are dramatically reduced, as compared to solutions obtained using all of the physically tractable lines available in the spectrum (the conventional approach[3]). To this end we make use of the same set of 133 lines used in the test calculations of Judge, Hubeny, & Brown (1997).

Finally, to go beyond a mere "proof of concept" for the usefulness of this GA-based technique, we turn our attention to extracting an optimal subset of observed lines from those in the wavelength range 280–1350 Å of the Harvard S-055 EUV Spectroheliometer (Reeves, Huber, & Timothy 1977). In § 4 we give the results of SELECTOR operating on the 40 strong lines available for this analysis (first order and lines significantly clear from blending effects) to obtain an optimal subset of 30 that increases the stability of any following numerical inversion. In addition, we make use of the average solar data tabulated by Vernazza & Reeves (1978), which provide an excellent test bed for inversions using optimal line subsets. We compare our results, for both optimal and full line sets, to those previously published in the literature, principally with Raymond & Doyle (1981b, hereafter RD1981b), but comparison may easily be made with Noyes et al. (1985) and Doyle et al. (1985).

2. PHYSICAL AND MATHEMATICAL BACKGROUND

2.1. *Modeling Line Emission Coefficients*

The foregoing discussion of optically thin line emission at or near coronal ionization equilibrium in a highly non-LTE plasma relies on the following assumptions (see, e.g., Mason & Monsignori-Fossi 1994):

1. The plasma is optically thin.
2. Atomic hydrogen, the major constituent, is fully ionized.
3. The electron velocity distribution is Maxwellian in nature.
4. The abundances of the elements in the plasma are constant.
5. Photoexcitation and stimulated emission can be neglected.

An analysis of the solar plasma carried out under these assumptions becomes similar to that of Pottasch (1964). Further, the total integrated line intensity (I_l) of a line, labeled l, is given by a double integral over n_e and T_e as first described by Jefferies, Orrall, & Zirker (1972a, 1972b), which takes the form

$$I_l = \int_{n_e}\int_{T_e} \frac{h\nu_l A_l}{4\pi} \frac{n_{u(l)}}{n_{\rm ion} n_e} \frac{n_{\rm ion}}{n_{el}} \frac{n_{el}}{n_{\rm H}} \frac{n_{\rm H}}{n_e} \times \mu(n_e, T_e) dn_e\, dT_e \ \text{ergs cm}^{-2}\ \text{sr}^{-1}\ \text{s}^{-1}\ . \quad (3)$$

Here A_l is the Einstein A-coefficient, $n_{u(l)}/n_{\rm ion} = f(n_e, T_e)$, $n_{\rm ion}/n_{el} = g(T_e)$, $n_{el}/n_{\rm H}$ and $n_{\rm H}/n_e$ are the relative population of the upper atomic level of the line, the ionic abundance, elemental abundance, and relative abundance of H to electrons (having a value of 0.8 in the solar atmosphere), respectively, and $\mu(n_e, T_e)$ is the bivariate differential emission measure of Judge et al. [1997; defined as $\Psi(n_e, T_e)$ by Brown et al. 1991 with $\Psi(n_e, T_e) = 4\pi S \mu(n_e, T_e)$ for projected emitting area S]. In essence $\mu(n_e, T_e)$ is a positive definite quantity measuring the volume distribution of emitting plasma differentially as a function of n_e and T_e within the plasma, weighted by n_e^2. From, Judge et al. (1997), the form of $\mu(n_e, T_e)$ is

$$\mu(n_e, T_e) = \oint_{L_{n_e,T_e}} \frac{n_e^2}{|n_e|\,|T_e|\,\sin\theta_{n_e,T_e}}\, dL_{n_e,T_e}\ \text{cm}^{-5}\ , \quad (4)$$

where θ_{n_e,T_e} (assumed to be nonzero) is the local angle between vectors ∇n_e and ∇T_e normal to surfaces S_{n_e}, S_{T_e} of constant electron density and temperature, respectively, and L_{n_e,T_e} is the line where the constant surfaces meet. The interested reader is referred to Figure 1 in Brown et al. (1991) for a perspective of the plasma geometry. Full descriptions of the other quantities in equation (3) can be found in Jordan (1969), Jacobs et al. (1977, 1980), and Arnaud & Rothenflug (1985).

At this point we choose to define the line emission coefficient $K_l(n_e, T_e)$ (normalized to n_e^2), hereafter simply referred to as the *emissivity*, as

$$K_l(n_e, T_e) = \frac{h\nu_l A_l}{4\pi} \frac{n_{u(l)}}{n_{\rm ion} n_e} \frac{n_{\rm ion}}{n_{el}} \frac{n_{el}}{n_{\rm H}} \frac{n_{\rm H}}{n_e}\ \text{ergs cm}^3\ \text{sr}^{-1}\ \text{s}^{-1}\ . \quad (5)$$

As discussed in Judge et al. (1997), the bivariate form of equation (3) is not easy to invert in a reliable manner. To make the most of this relationship it is often convenient to reduce it to an integral over a single variable by taking a moment of $\mu(n_e, T_e)$ with respect to n_e (see, e.g., McIntosh, Brown, & Judge 1998a), i.e.,

$$\xi(T_e) = \int_{n_e} \mu(n_e, T_e) dn_e\ \text{cm}^{-5}\ \text{K}^{-1}\ , \quad (6)$$

[3] What we refer to here as the "conventional method" consists of subjectively choosing emission lines for study primarily on their physical attributes and not necessarily on any mathematical basis. This in no way means that all of the lines observed are ultimately used in any inverse calculations; only the "good" lines are used.

noting that this equation is *equivalent* to the definition presented in equation (2). It is then straightforward to reduce equation (3) to a univariate form (integrating out the n_e dependence in the equation, cf. eq. [6] and assuming that we are operating in some fixed $n_e = n_0$ regime):

$$I_l = \int_{T_e} K_l(T_e)\xi(T_e)dT_e \,. \tag{7}$$

In formally solving equation (7) in §§ 3 and 4, we carry out the integration in terms of a logarithmic variable $t_e = \log_{10} T_e$, in order to facilitate the comparison of recovered DEMs to those published previously. This substitution leaves the structure of the governing equation unaffected:

$$I_l = \int_{t_e} K_l(t_e)\xi(t_e)dt_e \,, \tag{8}$$

where $\xi(t_e)$ is the DEM of $\log_{10} T_e$ (units of cm^{-5}). Once formed, univariate integrals, such as equation (7) or (8), contain all of the available information about the emitting optically thin plasma (Craig & Brown 1976) in terms of the T_e DEM function, $\xi(T_e)$ given that the assumptions made earlier are true. One can also take a moment of $\mu(n_e, T_e)$ with respect to T_e to yield an electron density DEM(see, e.g., McIntosh et al. 1998a or McIntosh 1998). In what follows we restrict ourselves to equation (8). Note that because the plasma is assumed to be optically thin, the integral over the line of sight has been totally "absorbed" in the integral over t_e; on the basis of the I_l's, two parcels of emitting plasma at different temperatures located at different locations along the line of sight *cannot* be distinguished from a single parcel of plasma containing two thermal components within the spatial resolution element characterizing the spectroscopic observation.

2.2. *The Condition Number*

We have previously observed that equation (8) takes the form of a Fredholm integral equation of the first kind for the differential emission measure in temperature. The solution of equation (8) will only reliably prescribe the form of $\xi(t_e)$ at one temperature point. Thus, to obtain a solution spanning our entire t_e domain we are required to make use of $N-1$ other lines such that we form a linear matrix system prescribing the discretized form of $\xi(t_e)$, $\boldsymbol{f} = [\xi(t_{e_1}), \ldots, \xi(t_{e_P})]$, at $P \leq N$ points (Craig & Brown 1986). In doing this, we have constructed a $(N \times P)$ matrix equation of the form

$$\boldsymbol{g} = \mathcal{K}\boldsymbol{f} \,, \tag{9}$$

where the data vector $\boldsymbol{g} = (I_1, \ldots, I_N)$ is comprised of line intensities and $\mathcal{K}$ is known as the *kernel matrix* and is the quantity with which determines the conditioning of the system. Notice that we explicitly assume that the elements of the kernel matrix are known exactly.

The form of equation (9) is overly simplified because, in general, there will be errors of significant magnitude ($\geq 10\%$) present in the observed line intensities. That is, we now anticipate a (vector) noise component $\delta\boldsymbol{g}$ in the data. This implies that the solution must then be represented by $\boldsymbol{f} = \boldsymbol{f}' + \delta\boldsymbol{f}$. It is easily shown that, for data errors such as these, we will observe error amplification through to the solution of the order (Craig & Brown 1986)

$$\frac{\| \delta\boldsymbol{f} \|}{\| \boldsymbol{f} \|} \leq \| \mathcal{K} \| \;\; \| \mathcal{K}^{-1} \| \, \frac{\| \delta\boldsymbol{g} \|}{\| \boldsymbol{g} \|} \,. \tag{10}$$

where $\| \boldsymbol{x} \|$ is the quadratic norm of $\boldsymbol{x}$. Now we can make use of the result that $\| \mathcal{K}^{-1} \| = \sigma_{\max}$, where $\sigma_{\max}$ is the maximum *singular value* of matrix $\mathcal{K}$ (these singular values are simply the eigenvalues of $\mathcal{K}^T\mathcal{K}$), and a corollary of this result to define the *condition number* C_K ($1 < C_K < \infty$) of the kernel matrix as

$$C_K = \| \mathcal{K} \| \;\; \| \mathcal{K}^{-1} \| = \frac{\sigma_{\max}}{\sigma_{\min}} \,, \tag{11}$$

where, the second equality arises since the singular values of $\mathcal{K}^{-1}$ are just the reciprocal singular values of $\mathcal{K}$ (see Golub & Van Loan 1989, § 2.5). Equation (11) indicates that the distributions of the singular values of $\mathcal{K}$ directly determines the level of error amplification to be expected in the solution of equation (9). Equation (11) immediately highlights the disastrous effect of zero (or near-zero) singular values, because these will dramatically increase C_K and have, in general, highly oscillatory (usually unphysical) eigenfunction counterparts (see the example on p. 9 of Craig & Brown 1986). These highly oscillatory functions, when multiplied by the reciprocal of a small number, dominate the behavior of any solution $\xi(t_e)$.

We therefore seek a *regularized* solution of equation (9). Classically this is performed by replacing $\mathcal{K}^{-1}$ by the appropriate *approximate inverse* $(\mathcal{K}^T\mathcal{K} + \Lambda\mathcal{H})^{-1}$ (Tichonov 1963; Louis 1996) and calculate the regularized solution $\boldsymbol{f}_\Lambda$ for the *smoothing parameter* Λ (≥ 0) and some a priori estimate of the functional form of the solution, e.g., a smooth nth derivative, represented by the *smoothing matrix* $\mathcal{H}$ as

$$\boldsymbol{f}_\Lambda = (\mathcal{K}^T\mathcal{K} + \Lambda\mathcal{H})^{-1}\mathcal{K}^T\boldsymbol{g} \,. \tag{12}$$

A detailed discussion of regularization is beyond the scope of this paper; we simply point out that it negates the effects that small singular values of $\mathcal{K}$ have on the solution by effectively replacing them by Λ (cf. eqs. [10] and [11]). The interested reader is referred to Tichonov (1963); Twomey (1963); Sneddon (1972); Craig & Brown (1986); Jin & Hou (1997) for in-depth discussion of particular regularization techniques. Unless otherwise stated, we perform inversions here using second-order regularization for a prescribed value of Λ.

The condition number is directly proportional to the degree of linear dependence in the rows of $\mathcal{K}$. This presents an obvious difficulty for the $\xi(t_e)$ problem, since using a large numbers of lines ensures that the "coverage" of the t_e domain is good, but the likelihood becomes high that some of these lines will have very similar kernels, leading to a high degree of linear dependence between some rows of $\mathcal{K}$, and so to a high value of C_K. Conversely, using fewer lines reduces the chance of ending up with nearly linearly dependent rows of $\mathcal{K}$, but increases the likelihood that some region in the t_e domain will be badly covered and so very poorly constrained by the data (see also Mariska 1992; Chap. 4). This brings us back to the nonuniqueness problem, since we are now in a situation where source functions $\xi(t_e)$ that look very different in the poorly covered region of the domain lead to the same data upon evaluating the right-hand-side of equation (8). This situation, from the point of view of the discretized system (eq. [9]), also leads to a high condition number! The requirements of low C_K and high coverage are in fundamental conflict.

These problem would obviously vanish if the emissivities closely resembled δ-functions or at least were well localized

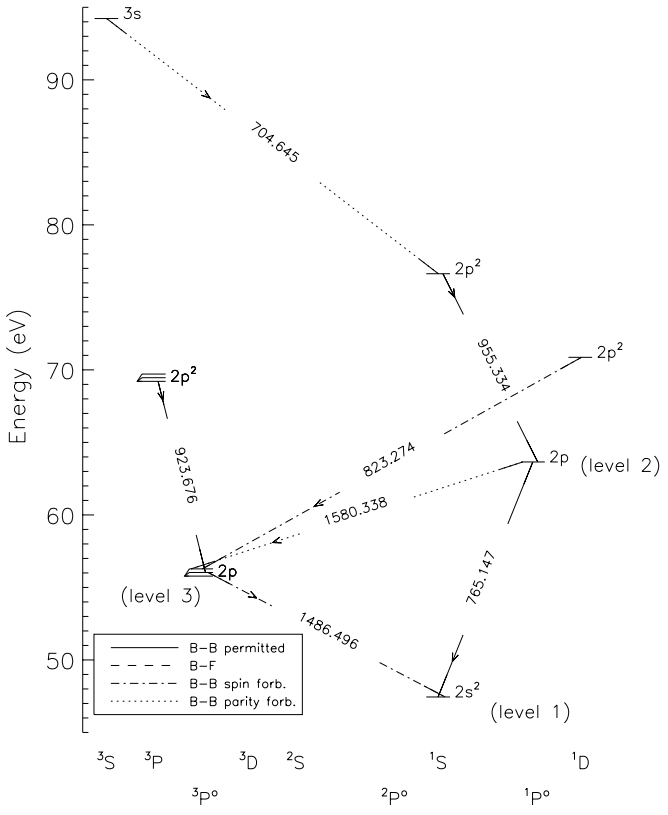

FIG. 1.—Term diagram of N IV for transitions with wavelengths less than 1600 Å. Indicated are the main lines of the ion including the 765.147 Å resonance line (*solid line*) and the 1486.496 Å intersystem line (*dot-dashed line*). The figure legend gives the nomenclature (and nature) of each transition, e.g., the 765.147 Å line is from a bound-bound permitted (in a quantum mechanical sense) transition, whereas the 1486.496 Å requires a spin change and is a bound-bound spin forbidden transition (its upper level is a long-lived *metastable* level). The lower three levels (i.e., those below 65 eV indicated [levels 1, 2, and 3]) can be considered as forming a simple three-level atom. The Horizontal axis is sorted according to the angular momentum quantum number (L). These data are extracted from the HAOS-diaper software package (Judge & Meisner 1994).

in t_e space. Unfortunately, the emissivities that form the rows of the kernel matrix are not ideal and have a finite amount of spread, dependent on the line formation parameters. We now discuss the form of this spread.

2.3. *Physical Nature of the Kernels*

To discuss the functional behavior of certain emission lines we must consider the form of equation (5) as a function of n_e and T_e. For illustration purposes we consider a simple three-level atom with level 3 metastable,[4] like that presented in Figure 1 for N IV. Upon solving for non-LTE statistical equilibrium for our hypothetical atom we obtain the population densities for levels 2 (n_2) and 3 (n_3) in terms of the population density of the ground level (n_1). For the *resonance* line (transition from level 2 to the level 1, see, e.g., the 765.15 Å transition—*solid line*—in Fig. 1) we have, assuming the population of level 3 to be negligible,

$$n_2 = \frac{n_e n_1 C_{12}}{A_{21}}, \tag{13}$$

[4] While restricted, this picture illustrates all the important physical processes that determine K_l. In practice, detailed multilevel calculations are performed.

giving an emissivity $[K_{\rm res}(n_e, T_e)]$ of the form

$$K_{\rm res}(n_e, T_e) = \frac{h\nu_{12} C_{12}}{4\pi} \frac{n_1}{n_{\rm ion}} \frac{n_{\rm ion}}{n_{el}} \frac{n_{el}}{n_{\rm H}} \frac{n_{\rm H}}{n_e}. \tag{14}$$

An *intersystem* line (transition from level 3 to level 1; the 1486.50 Å transition—*dot-dashed line*—in Fig. 1), involving the population density of the metastable level 3,

$$n_3 = \frac{n_e n_1 C_{13}}{A_{31} + n_e(C_{31} + C_{32})}, \tag{15}$$

will have an emissivity $[K_{\rm int}(n_e, T_e)]$ behaving as

$$K_{\rm int}(n_e, T_e) = \frac{h\nu_{31}}{4\pi} \left\{ C_{13} \left[1 + \frac{n_e(C_{31} + C_{32})}{A_{31}} \right]^{-1} \right\} \times \frac{n_1}{n_{\rm ion}} \frac{n_{\rm ion}}{n_{el}} \frac{n_{el}}{n_{\rm H}} \frac{n_{\rm H}}{n_e}. \tag{16}$$

where $C_{ji} = g_j^{-1} \kappa \Upsilon_{ji}(T_e) T_e^{-1/2}$ $(j > i)$ is the collisional excitation coefficient (units of s^{-1}) with the statistical weight of the upper level g_j, $\Upsilon_{ji}(T_e)$ is the Maxwellian averaged collision strength and κ is a numerical constant. The functional behavior of all the emissivities we will consider can be categorized as belonging to one or the other of these two classes. In this non-LTE plasma regime the electrons are assumed to belong to a Maxwell-Boltzmann distribution and populate the ground level preferentially. Such simplifications mean that C_{ij} is treated strictly a function of T_e. Indeed, at this point we can categorically state the following:

1. The assumption of a Maxwellian electron distribution ensures that, because of ionization equilibrium, $K_l(n_e, T_e)$ will be approximately Gaussian in the T_e domain or, more exactly, peaked around the temperature of maximum formation of the ionic stage to which that transition belongs, with a full width at half-maximum of 0.3 in t_e (see, e.g., Jordan & Wilson 1971). There are *small* departures from this peak temperature arising from the contributions of the other factors in equations (14) and (16).
2. All lines will emit irrespective of the electron density of the plasma. Therefore, $K_l(n_e, T_e)$ will cover the entire $n_e(10^8$–10^{12} cm$^{-3})$ domain of the upper solar atmosphere, but their functional behavior will depend critically on the transition from which they arise.

For a resonance line in the simple three-level atom (see, e.g., Fig. 1), with n_e constant ($n_0 = 10^9$ cm^{-3}), inspection of equation (14) will show that the functional dependence of $K_{\rm res}(T_e)$ is determined by the interplay between the population of the ground level (itself dependent on the abundance of the ionization stage to which the transition belongs) and the collisional excitation rate of the transition. The approximation of a Maxwellian-Boltzmann electron distribution will ensure that $K_{\rm res}(T_e)$ is a peaked function of T_e with its maximum at some temperature T_0, the value of T_e, where the ionic abundance is a maximum for this particular n_0. This behavior is clear on inspection of the solid line in Figure 2, a plot of the emissivity of the N IV 765.15 Å resonance line.

As can be appreciated from equation (16), the T_e dependence of an intersystem line's emissivity is not quite as trivial. Equation (16) shows that the critical electron density n_{e_c} (where $n_e C_{23} \approx A_{31}$) plays an important role. The value of n_{e_c} is different for each transition. If we have for a particu-

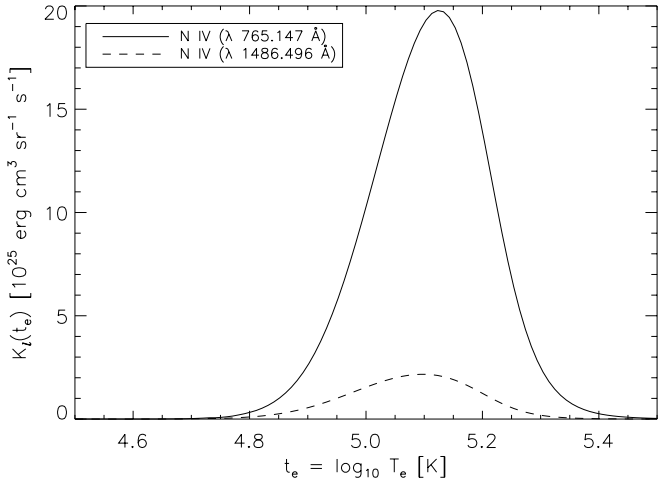

FIG. 2.—Emissivities of a resonance line (*solid line*) and intersystem line (*dashed line*) as functions of temperature only. These are for lines of N IV (wavelengths 765.147, 1486.496 Å) calculated for a electron density of 10^9 cm^{-3}. These data are extracted from the HAOS-diaper software package (Judge & Meisner 1994).

lar intersystem transition the case where $n_0 \ll n_{e_c}$ the temperature dependence of $K_{\rm int}(T_e)$ will be determined solely by the numerator and will resemble $K_{\rm res}(T_e)$ and be a strongly peaked function. However, another intersystem transition may depend on a metastable level which has $n_0 > n_{c_e}$ and then both the denominator and numerator must be considered as important terms. $K_{\rm res}(T_e)$ (at this fixed density $n_0 > n_{c_e}$) can be approximated from the collision strengths (Υ_{31} and Υ_{32}) and the other ratio factors (indicated below as [...]) present for the relevant transition in equation (16) by

$$K_{\rm int}(T_e) \approx \frac{g_3}{g_1} \frac{\Upsilon_{31}(T_e) \exp\left(-E_{13}/k_{\rm B}\, T_e\right)}{\Upsilon_{31}(T_e) + \Upsilon_{32}(T_e)} [\ldots] , \quad (17)$$

where E_{13} is the transition energy and $k_{\rm B}$ is Boltzmann's coefficient. The resulting function has a roughly Gaussian shape, peaked at the temperature of maximum ionic abundance, but skewed shortward of T_0. Again, this is clearly observed in the dot-dashed line of Figure 2, where we show the emissivity of the intersystem line N IV at 1486.50 Å.

The emissivities used in what follows belong to strong transitions in the wavelength range 150–1610 Å for ions of various isoelectronic sequences from atoms including: carbon (C II–C IV), iron (Fe XII–Fe XV), magnesium (Mg VI–Mg X), neon (Ne VI–Ne VIII), nitrogen (N II–N V), oxygen (O II–O VI), and silicon (Si III–Si XII). The precise details of the isoelectronic transitions used are given in Table 1, and there are 133 lines in total. In Figure 3 we plot the singular value distribution for a kernel matrix composed of these 133 lines which we will refer to, from now on, as the "All-lines" kernel. It has a condition number, determined by equation (11), of $\log_{10} C_K = 5.9470$. It is worth pausing to reflect on what this implies; as per equation (10), relative data error $\| \delta \boldsymbol{g} \| / \| \boldsymbol{g} \|$ will be amplified by a factor $\simeq 10^6$! The only way to prevent the occurrence of unphysical oscillations in $\boldsymbol{f}$ is then to impose strong regularization. In doing so however, one loses the ability to recover sharp physical structures in the source function $\xi(t_e)$. This

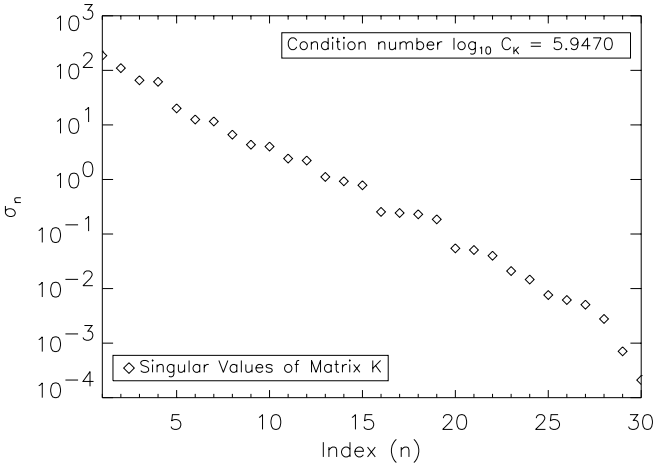

FIG. 3.—Singular value (σ_n) distribution of the matrix constructed from *all* $N = 133$ line emissivities considered for the $\xi(t_e)$ inverse problem with a $P = 30$ point discretization. The condition number is given by the ratio of the largest to smallest singular value.

TABLE 1

TRANSITION CONFIGURATIONS OF THE (SYNTHETIC) EMISSION LINES USED TO PRODUCE THE EMISSIVITIES FOR §§ 2.6 AND 3

Isoelectronic Sequence	Transitions	Ions
Lithium	$2s$–$2p$, $2s$–$3p$	C IV, N V, O VI, Ne VIII, Mg X, Si XII
Beryllium	$2s^2\ S$–$2s2p\ ^3P$, ^1P	C III, N IV, O V, Ne VII, Mg IX, Si XI
	$2s2p\ P3$, ^1P–$2p^2\ ^3P$, ^1D, ^1S	
Boron	$2s^22p\ P$–$2s2p^2\ ^4P$, ^2D	C II, N III, O IV, Ne VI, Mg VIII, Si X
	$2s2p^2\ P$–$2p^3\ ^4S$	
Carbon	$2s^22p^2\ P$–$2s2p\ ^3\ ^5S$, ^3D	O III, Mg VII, Si IX
	$2s^22p^2\ P$–$2s^2\ 2p^2\ ^1D$, ^1S	
	$2s^22p^2\ D$–$2s2p\ ^3\ ^1P$, ^1D	
Nitrogen	$2p^3\ S$–$2p^23s\ ^4P$	O II, Mg VI
Sodium	$3s$–$3p$	Si IV
Magnesium	$3s^2\ S$–$3s3p\ ^3P$, ^1P	Si III
	$3s3p^2\ P$–$3p^2\ ^3P$	

NOTES.—Transition configurations of the (synthetic) emission lines used to produce the emissivities for §§ 2.6 and 3 of this paper. Only lines in the range of the CDS and SUMER instruments on *SOHO* were used (150–1610 Å). Seven high electronic sequence lines from the iron ions Fe XII–Fe XV (not listed) are also used.

loss of information is clearly something to be avoided as much as possible (see, e.g., Kashyap & Drake 1998).

2.4. *Line Selection as a Combinatorial Optimization Problem*

In view of the above considerations regarding the ill conditioning of the DEM inverse problem, it would appear advantageous to set up the inversion problem in a manner that minimizes error amplification, i.e., that minimizes C_K. This can be achieved in principle by carrying out the inversion using only a subset of lines with minimally overlapping kernels, while maintaining a reasonable coverage in source function space. How should one go about choosing an adequate subset of lines that strikes a proper balance between these two conflicting requirements? Physical insight into the atomic physics underlying the nature of the kernels can help, but if a great many lines are available, such an approach may not yield near-optimal results.

In essence, we are facing a combinatorial optimization problem. Given a (large) set of N emission lines, we seek the subset of M ($<N$) lines that minimizes the condition number C_K. Recall that the number of possible combinations of M distinct objects drawn from a larger set of N objects is given by

$$(NM) = \frac{N!}{M!(N-M)!} \tag{18}$$

For our application, this will be a very large number. Consider for example the task of finding the best set of 30 lines out the 133 used by the "HAOS-diaper" software package (Judge & Meisner 1994). There are approximately 10^{29} such combinations, far too many for enumeration or Monte Carlo search to even be an option. Moreover, precisely because many lines have similar kernels, this combinatorial problem can be expected to be strongly multimodal, in that many different sets of lines can lead to similar C_K. In other words, the search space is not only immense, it also contains a great many secondary minima. The optimization problem we are contemplating is clearly a hard one.

Fortunately, we are not strictly required to find the *absolute best* of all 10^{29} possible line combinations, but rather one line combination that leads to a low enough C_K. This opens the possibility of using heuristic search techniques that, while not necessarily finding the absolute minimum in search space, will produce a solution "good enough, fast enough." We adopt such an approach here, based on the class of evolutionary algorithms known as genetic algorithms (GA; Holland 1962; Goldberg 1989; Mitchell 1996).

2.5. *SELECTOR: A Genetic Algorithm-based Combinatorial Optimizer*

First define a trial solution as a list of M distinct emission lines. A GA searches for the best possible solution via the following iterative steps:

1. [Initialization] Construct a population of trial solutions, where each solution consists of a *randomly* selected subset of M lines.
2. [Begin Iteration] For each population member, construct the corresponding DEM kernel and calculate C_K.
3. Rank the population according to condition number; low C_K means high "fitness."
4. Select and breed the subset of population members with higher fitness.
5. Replace population by newly bred trial solutions.
6. If termination criterion not reached, then return to step 2, else proceed.
7. [End Iteration] Return the trial solution with the lowest C_K in the current population as the set of UV/EUV lines that minimizes the condition number of the kernel matrix.

Breeding, which is what gives GA its name, is carried out by encoding selected pairs of trial solutions as strings that uniquely identify the set of M distinct lines associated with each solution. Those strings are then subjected to biologically inspired operations of crossover and mutation. The details of these operations need not concern us here (see Charbonneau 1995 for a gentle introduction). Let us simply mention that the encoding scheme and operators must be such that "offspring" solutions retain some of the features (i.e., subset of lines) that gave their "parents" a low enough C_K to be selected for breeding in the first place, while producing novel combinations of lines. This very triad, fitness-based selection + inheritance + variation, is in fact at the very core of the biological evolutionary process. For a fixed selection criterion (here, the lower C_K the better), over sufficiently many algorithmic iteration a lowering of the fittest population member's C_K is basically unavoidable. On the other hand, for a large, hard problem it is quite likely that the GA will not find the absolute lowest possible C_K in a computationally reasonable number of generational iterations. Recall, however, that this is not we are trying to achieve; we are only interested in finding a line subset that yields a low enough C_K.

Our SELECTOR algorithm makes use of a modified version of the GA-based optimization subroutine PIKAIA, described in Charbonneau & Knapp (1996; see also the Appendix of Charbonneau 1995). The modifications are needed to ensure that the action of the crossover and mutation operations on the strings defining parent solutions leads to most parent lines being passed to the offspring solutions, without producing duplicate lines in either offspring. This can be achieved by a variation on the so-called ordinal representation scheme (see, e.g., Michalewicz 1994, § 10). Details of this modified scheme will be presented elsewhere (McIntosh & Charbonneau 2000).

Because the scheme is an iterative method working on a population of trial solutions, in general a large number of solutions will be evaluated in the course of the evolutionary process. Each such evaluation involves (a) the construction of the kernel matrix, defined by equation (9), and (b) the calculation of its condition number. The second step can be performed by singular value decomposition (SVD; see for example Press et al. 1992, § 2.6), but this is a relatively demanding computational task. In what follow we make use of a much faster technique due to Clive et al. (1979), which we found provides a reasonably accurate *estimate* of the condition number, provided that we have $M = P$ (i.e., a square problem).

2.6. *SELECTOR's Performance*

In light of our previous discussion about the expected mathematical and physical form of a well-conditioned kernel matrix, let us first define two quantities that will prove useful for the foregoing analysis. In order to be able to measure how well the temperature domain is being covered by the selected emissivities that constitute the

kernel matrix, we define the normalized linear superposition kernel $S(t_e)$ as

$$S(t_e) = \sum_{l=1}^{M} K_l^*(t_e) , \tag{19}$$

$$\hat{S}(t_e) = \frac{S(t_e)}{\text{Max } [S(t_e)]} , \tag{20}$$

where $K_l^*(t_e)$ is the normalized emissivity of the line labeled l and M is the number of lines used in the calculation. The second quantity we introduce is the fractional coverage of any kernel matrix, f, as the integral of equation (20) over the entire t_e domain, i.e.,

$$f = \frac{1}{P} \int_{t_e} \hat{S}(t_e) dt_e \tag{21}$$

where P is the number of points over which the temperature domain is discretized ($P = 30$ for the calculations reported below).

In Figure 4 we use these quantities to illustrate the evolutionary behavior of a single 2000 generation SELECTOR run. Figure 4*a* shows the evolving shape of $S(t_e)$, for generations $j = \{1, 250, 500, 1000, 2000\}$. Only the fittest individual of each of those generations is plotted. Note the evolution to a state where the superposition of the emissivities gradually span the t_e domain with increased uniformity. This evidently leads to a gradual increase in fractional coverage f and is accompanied by a decrease of the condition number, as can be seen in Figure 4*b* (again only the best individual at each generation is plotted). After 2000 generations C_K has fallen to $\log_{10} C_K = 4.9640$. Recall that the condition number corresponding to the "All-lines" approach, on the other hand, is $\log_{10} C_K = 5.9470$.

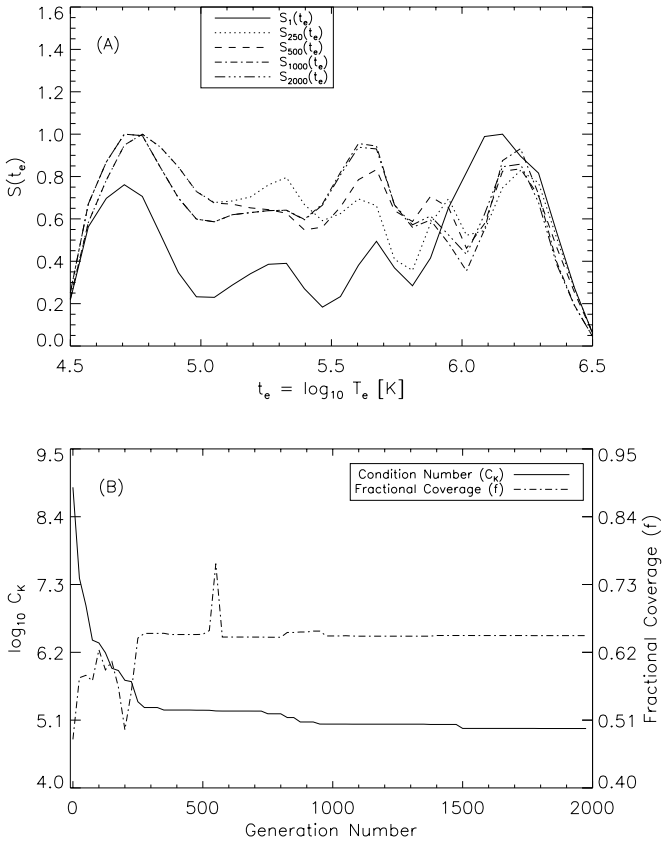

FIG. 4.—Variation of the coverage and condition number in the course of an evolutionary run. Panel (*a*) superimposes plots of $S(t_e)$ at generation $j = \{1, 250, 500, 1000, 2000\}$ during a typical SELECTOR evolutionary run. Panel (*b*) shows the fractional coverage f (*dot-dashed line*) of the best solution in the population and its condition number (*solid line*) at every generation. Better conditioned kernels have a more uniform coverage over the entire t_e domain.

After a few hundred generations, the later evolutionary phases are characterized by relatively long periods of stasis, where often both f and C_K remain constant, interrupted by short-lived epochs of abrupt decrease in C_K. Such evolutionary "jumps" are not a mere consequence of the discrete, combinatorial nature of the problem; they are a generic trademark of GA optimization. They occur when breeding generates a novel, higher than average line combination that spreads through the population in subsequent generational iterations.

It is quite striking that the net fractional coverage only increases slightly, from about 50% to 65% in the course of the complete run. This is hardly better than the "All-lines" coverage of $f = 0.614$. However, the condition number falls by over 4 orders of magnitude. This indicates that while many different line combinations can add up to essentially the same coverage, some of them are clearly superior to others in term of C_K. *Homogeneous coverage, in itself, is not a reliable measure of conditioning and does not guarantee a numerically stable inversion.*

Figure 5 shows the distribution of condition numbers (Fig. 5*a*, *thicker line*) and fractional coverage (Fig. 5*b*) resulting from running SELECTOR 300 times (5000 generation runs). The distribution is quite narrow, indicating that SELECTOR reliably finds solutions with condition numbers $C_K \sim 10^5$, a factor of 10 smaller than for the "All-lines" approach (which leads to $\log_{10} C_K = 5.9470$), and significantly better fractional coverage. Examination of the evolutionary runs also reveals that by 2000 generations the condition number is already within a factor of 2 of its final value attained after 5000 generations.

How much of this is a mere results of having reduced the number of lines from 133 to 30? This can be answered by repeatedly selecting randomly 30 lines from the 133 available, and computing C_K and f. The results of this purely random approach are disastrous: an average $C_K \sim 10^{10}$ and fractional coverage $f \sim 0.456$. Proper line selection is clearly not a trivial business.

A computationally fairer Monte Carlo approach would be to produce as many random sets of 30 lines as are evaluated in the course of a SELECTOR run (here 5×10^5; population size 100 times 5000 generations), and retain the single best line combination so produced. The thin lines on Figure 5 shows the distribution of C_K and f resulting from this new Monte Carlo procedure. The average C_K is still nearly 3 orders of magnitude larger than that found by SELECTOR for the same amount of computation, and fractional coverage is significantly poorer. The mean of the Monte Carlo distribution is $\log_{10} C_K = 7.8094$ (with extrema 7.2701 and 12.195), much higher than that of the "All-lines" C_K, while the mean of the SELECTOR distribution is $\log_{10} C_K = 4.9086$ (with extrema of 4.8034 and 5.1269), an order of magnitude lower than the "All-lines" C_K.

As alluded to earlier the condition number of the matrix arising from the discretization of equation (8) represents a trade-off between the degree of linear dependence in the

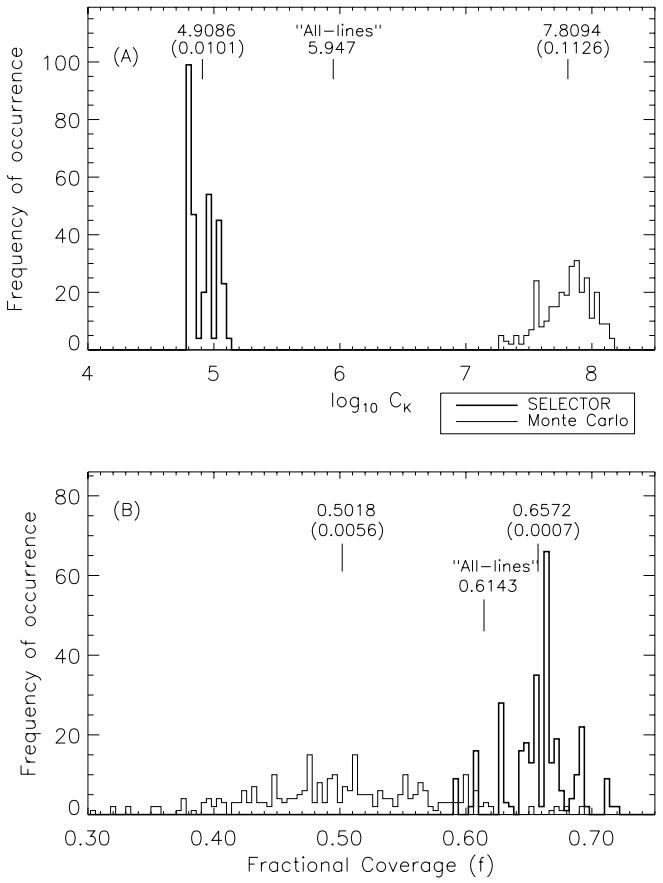

FIG. 5.—Distributions from the 300 run ensembles of SELECTOR (*thick solid line*) and iterated Monte Carlo search algorithm (*thin solid line*). The quantities listed along the top edge of each panel are distribution mean condition numbers (also indicated by the vertical tick marks) and variances (in parenthesis) for each distribution. Note the position of the "All-lines" C_K relative to the two distributions.

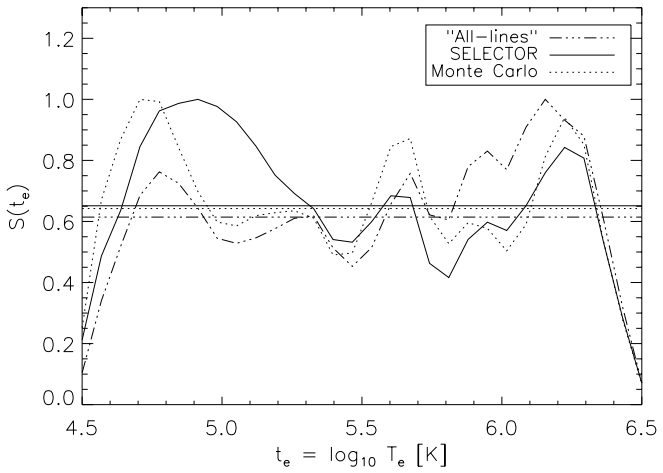

FIG. 6.—Normalized linear superposition kernel $S(t_e)$ for the "All-lines" kernel (*dot-dashed line*), the optimal SELECTOR kernel (*solid line*), and iterated Monte Carlo search algorithm (*dotted line*). The horizontal lines represent the value of fractional coverage (f) for each of the above.

rows and how well the functional domain (here $t_e = \log_{10} T_e$) is covered. The fact that nearly all combinations of 30 lines lead to a significantly higher C_K than if 133 lines are used indicates that coverage is here an important determinant of C_K, since one would expect that the "All-lines" kernel should be characterized by a larger number of nearly linearly dependent rows (cf. lines of the same ion will peak at roughly the same temperature). In Figure 6 we show this coverage effect by plotting $S(t_e)$ for the lines belonging to the runs of SELECTOR (*solid line*) and Monte Carlo (*dashed line*) against that of the "All-lines" kernel (*dot-dashed line*).

In Figure 7 we show a line selection histogram constructed on the basis of multiple, independent SELECTOR runs. It is clear that some lines are chosen significantly more often than others. The figure, however, gives no clear indication that *any* of these lines occur together in the sets chosen, or in separate subsets, to form a kernel of significantly lower condition number. In fact, the condition number of the kernel matrix formed by the 30 lines selected most often is quite high, namely $\log_{10} C_K = 7.3585$. This highlights the multimodal nature of the combinatorial optimization problem presented by line selection (cf. discussion in § 2.5).

The data from Figure 7 are collated in Table 2. There we provide the details of all the lines appearing in Figure 7 that have selection frequencies above the mean (67.7). Also given are the temperatures ($t_e^{\max}$) at which $K_l(t_e)$ peaks. Lines belonging to the set with the smallest C_K are indicated by an asterisk (*). In Table 3 we give the details of the line the optimal set of 30 lines.

In conclusion, we can state that selecting only a subset of available emission lines can lead to a better conditioned discretized system only if the selection is carried out in such a way as to explicitly minimize the condition number.[5] In the next section we explore the consequences of this form of

[5] In practice, a true preconditioning step to the *observation* of UV/EUV lines would encompass the mathematics (C_K minimization), atomic physics (t_e coverage of the kernels) and the observational limitations (instrumental capabilities, calibration, etc.) of individual lines as one. However, in this section we assume that the UV/EUV lines are all observable and then use SELECTOR to extract those to be retained for the numerical inversion.

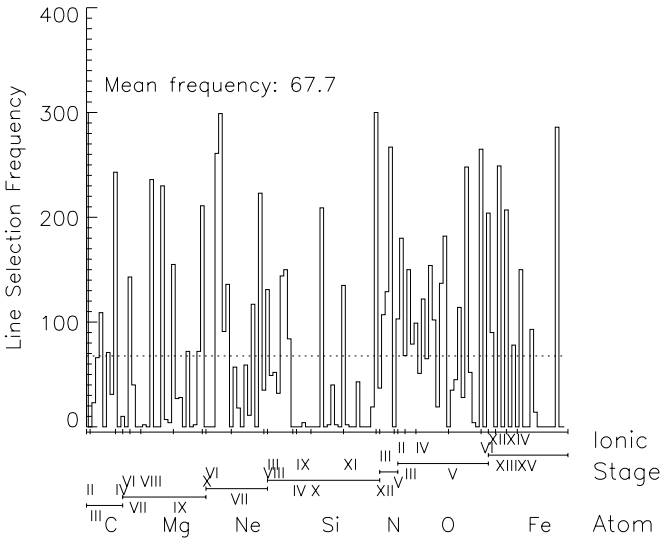

FIG. 7.—Histogram of line selection frequency for 300 runs of SELECTOR. The lower axis identifies the atom (large division) and ionization stage (corresponding to the small division label) to which each line belongs. Notice the existence of a subset of the 133 lines that have selection frequencies significantly greater than the mean of 67.7. However, these do not form *the* optimal subset of 30 lines; using the 30 most frequently selected lines yields $\log_{10} C_K = 7.3586$, much larger than for the "All-lines" kernel.

TABLE 2

DETAILS OF THE EMISSION LINES SELECTED MOST AT THE END OF THE 300 5000 GENERATION RUNS OF SELECTOR

Ion	λ (Å)	Count	t_e^{max}	Ion	λ (Å)	Count	t_e^{max}
C II	1335.66	300	4.568*	C III	1175.59	109	4.844*
C III	1175.98	71	4.844*	C IV	312.420	243	5.051*
Mg VII	431.188	143	5.741	Mg VIII.....	436.671	236	5.879*
Mg VIII.....	772.749	230	5.879*	Mg IX	443.972	72	5.948
Mg IX	368.070	155	5.948*	Mg IX	706.060	72	5.948
Mg X	609.793	211	6.017*	Ne VI.....	562.711	261	5.603*
Ne VI.....	999.630	299	5.534*	Ne VI.....	1006.09	91	5.534
Ne VI.....	1010.60	136	5.603	Ne VII	564.528	117	5.672*
Ne VII	895.175	223	5.672*	Si III	1206.49	131	4.706*
Si III	1298.94	144	4.706*	Si III	1301.14	150	4.706
Si III	1303.32	84	4.706	N III	771.900	107	4.913
N III	772.385	129	4.913*	N III	991.502	267	4.913*
O II.....	539.085	180	4.637	O II.....	540.005	103	4.637
O III	833.715	68	4.844*	O III	1660.80	150	4.844*
O III	1666.14	79	4.844	O IV	624.618	99	5.189
O IV	625.852	122	5.189	O IV	1397.23	154	5.120
O IV	1399.78	102	5.189	O IV	1404.80	137	5.189*
O IV	1407.38	182	5.189*	O V.....	761.128	248	5.327*
O V.....	760.227	114	5.327*	O VI	150.089	265	5.465*
Si X.....	356.050	209	6.086*	Si XI	303.582	135	6.155
Si XII	499.405	300	6.224*	Fe XII	1242.00	204	6.086*
Fe XIII.....	1216.46	249	6.224*	Fe XIV.....	334.172	207	6.263*
Fe XIV.....	447.329	78	6.263	Fe XV	281.342	150	6.293*
Fe XV	300.351	93	6.293	Fe XV	419.552	286	6.293*

NOTES.—The emission lines included here are those with selection frequencies greater than the mean of 67.7 counts. The lines indicated by an asterisk (*) are those belonging the set having the minimum value of $\log_{10} C_K = 4.8034$. Also given are the ions to which the line belongs, wavelengths λ (Å), the number of times the line was selected and the temperature ($t_e = \log_{10} T_e$) at with the emissivity of the line peaks, t_e^{max}.

preconditioning for the stability of the numerical solutions obtained by regularized inversion with synthetic data. In § 4 we will perform the same condition number optimization for a set of 40 lines observed by the *Skylab* Harvard S-055 Spectroheliometer (Reeves, Huber, & Timothy 1977) to validate this preconditioning step and show that it can improve the numerical stability of inversions using "real" data.

3. RESULTS ON SYNTHETIC LINE INTENSITIES

The majority of publications presenting derivations of DEM distributions $\xi(T_e)$ [or $\xi(t_e)$, with $t_e = \log_{10} T_e$] from

TABLE 3

DETAILS OF THE OPTIMAL SUBSET OF EMISSION LINES ONLY

Ion	λ (Å)	Count	t_e^{max}	Ion	λ (Å)	Count	t_e^{max}
C II	1335.66	300	4.568	C III	1175.98	71	4.844
C IV	312.420	243	5.051	Mg VIII.....	436.671	236	5.879
Mg VIII.....	772.749	230	5.879	Mg IX	368.070	155	5.948
Mg X	609.793	211	6.017	Ne VI.....	562.711	261	5.603
Ne VI.....	999.630	299	5.534	Ne VII	564.528	117	5.672
Ne VII	895.175	223	5.672	Si III	1206.49	131	4.706
Si III	1298.94	144	4.706	N III	772.385	129	4.913
N III	991.502	267	4.913	O III	833.715	68	4.844
O III	1660.80	150	4.844	O IV	625.127	51	5.120
O IV	1404.80	137	5.189	O IV	1407.38	182	5.189
O V.....	760.227	114	5.327	O V.....	761.128	248	5.327
O VI	150.089	265	5.465	Si X.....	356.050	209	6.086
Si XII	499.405	300	6.224	Fe XII	1242.00	204	6.086
Fe XIII.....	1216.46	249	6.224	Fe XIV.....	334.172	207	6.224
Fe XV	281.342	150	6.293	Fe XV	419.552	286	6.293

NOTES.—These are the lines belonging to the SELECTOR run that form a kernel matrix with $\log_{10} C_K = 4.8034$. Given are the ions to which the line belongs, wavelengths λ (Å), the number of times the particular line was selected and the temperature ($t_e = \log_{10} T_e$) at with the emissivity of the line peaks, t_e^{max}.

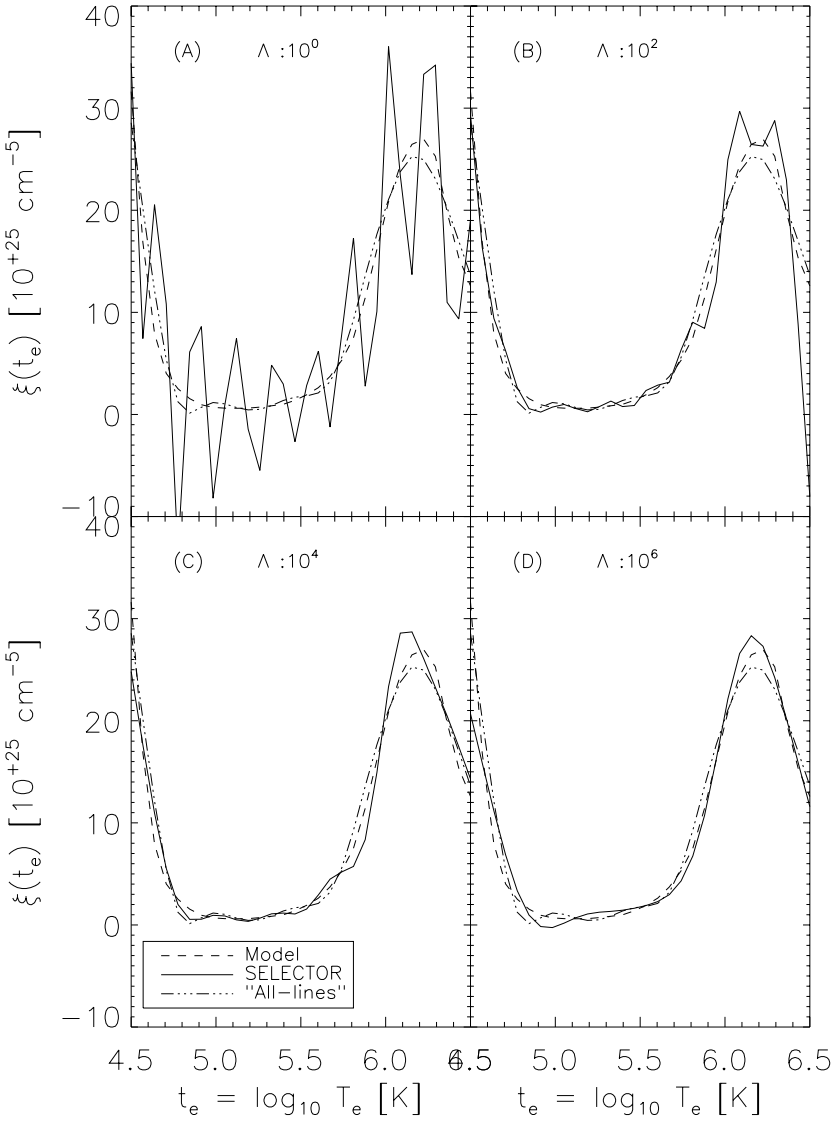

FIG. 8.—Regularized inversion (for smoothing parameters, Λ, varying from 10^0 to 10^6) of line intensities calculated for a model $\xi(t_e)$ function (*dashed line*). The SELECTOR $\xi(t_e)$ function recovered (*solid line*) is clearly more numerically stable than that for the "All-lines" (*dot-dashed line*) approach in the presence of errors in the line intensities. The line intensities used in these inversions have normally uniformly errors of relative magnitude $\pm 15\%$. It is clear that physical (positive definite) solutions exist for smaller values of Λ for the SELECTOR $\xi(t_e)$ inversions, in this case Λ has to be 10^6 in the "All-lines" inversion before we recover a physical solution compared to 10^2 for the SELECTOR case.

observed UV/EUV line intensities from the Sun or other stars adopt what we have called here the "All-lines" approach (see, e.g., Kashyap & Drake 1998; Lanzafame et al. 2000). This method involves making a physically subjective line choice from *every* emission line observed to construct the kernel matrix ($\mathscr{K}$) for the inverse problem and hence perform the numerical inversion and obtain $\xi(t_e)$ (as stated in footnote 3). In most of these works the effect of error propagation from data to solution associated with the poor conditioning of the discretized integral operator has seldom been given proper consideration (in our opinion). Consequently, we use the selection algorithm described in the previous section as a *preconditioning step* to the inversion calculation proper. As will become apparent below, choosing a subset of available emission lines on a more mathematical basis leads to an inversion that exhibits much better numerical stability than in the "All-line" case while also satisfying the physical criteria imposed. We must stress that the analysis of this section is on a "proof of concept" basis and ignores the distinct possibility that some of the 133 lines used maybe very weak in the solar UV/EUV spectrum (possibly blended or unobservable; C. Jordan 1999, private communication). We will consider the case of true observed lines in the following section.

With the results of the preceding section at hand, we perform inversions for both the optimal subset of 30 SUMER/CDS lines (specifically, those obtained by the SELECTOR run with the lowest final value of C_K), as well as the full set of 133 emission lines (taken from Judge et al. 1997), in order to compare the stability of the corresponding solutions. These inversions make use of $P = 30$ discretization points uniformly distributed in t_e and are performed using a regularization "forward-backward" method. This method involves computation of line intensities (with uniformly distributed errors in the range $\pm 15\%$) for a given model $\xi(t_e)$ function. The model we have used is

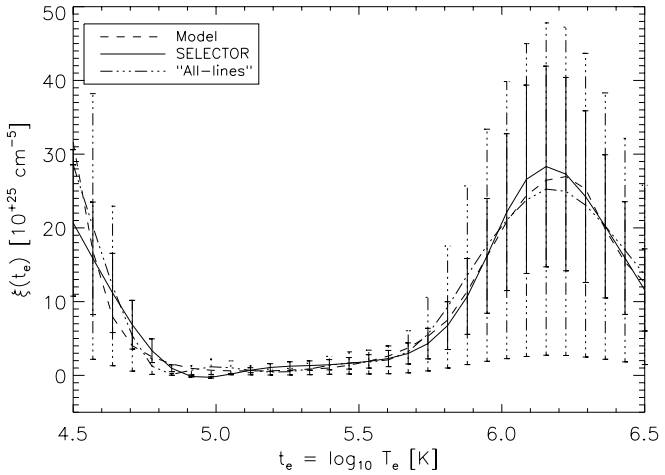

FIG. 9.—Inversions from Fig. 8*d* for the model $\xi(t_e)$ function (*dashed line*) with $\Lambda = 10^6$. Now included are the formal error bars for each solution, the SELECTOR $\xi(t_e)$ function (*solid line*) and the "All-lines" case (*dot-dashed line*). These error bars decrease with decreasing Λ, but this is accompanied by a decreased stability of the numerical solution (see Fig. 8). The SELECTOR-preconditioned solution is not only more stable with respect to variations in Λ, it also yields significantly smaller formal error bars at a given value of Λ. To bring the error bars on the "All-lines" solution down to comparable magnitude requires Λ to be reduced by 4 orders of magnitude; however, the solution is then very unstable numerically (see Fig. 8*b*).

the average quiet-Sun $\xi(t_e)$ taken from Figure 3 of RD1981b.[6] It is then a simple case of employing a second-order Tichonov regularization algorithm like that discussed in § 2 with a range of smoothing parameters Λ (10^0–10^6) to obtain a solution.

In Figure 8 we present the inversions for the synthetic line intensities [from our chosen model $\xi(t_e)$; *dashed line*] for a wide range of smoothing parameters (10^0–10^6) for the optimal subset (*solid line*), as well as the "All-lines" case (*dot-dashed line*). From Figures 8*a*–8*d* it is clear that the inversion performed with the optimal subset of lines has a significantly greater degree of numerical stability for a given value of Λ. We also note that to achieve a stable physical (positive definite) solution from the "All-lines" case requires that we use a large value of Λ; such increases in Λ will jeopardize the recovery of structure in the inferred $\xi(t_e)$ because regularization will flatten indiscriminately numerical oscillations as well as physically meaningful sharp features.

Using the optimal line set allows us to impose much smaller values of Λ (4 orders of magnitude) to achieve a stable (positive definite) solution,[7] which will also lead to smaller error bars on the inferred solution. The error bars returned by the inversion scheme are formal error estimates that measure the residual discrepancies, in a least-squares sense, between the right- and left-hand sides of equation (7). Weak regularization allows us to fit the data better (in a formal sense), even though what is being fitted is to a large degree data noise; from a physical point of view, the inferred solution is then not particularly accurate or even meaningful. Increasing regularization decreases the quality of the fit, leading to larger formal error bars.

This phenomenon is illustrated on Figure 9, which replicates Figure 8*d* but now includes error estimates returned by the inversion. Within its 1 σ error bars, the "All-lines" solution is consistent with a flat $\xi(t_e)$ for $t_e \geq 5.5$. The SELECTOR-preconditioned solution, on the other hand, provides a statistically significant measure of the maximum at $t_e \approx 6.2$. This demonstrates that an inversion using the optimal line set is more likely to recover physical structure in a statistically meaningful manner.

4. APPLICATION TO *SKYLAB* S-055 SPECTROHELIOMETER DATA

The analysis of the previous section concentrated on using the optimal line set obtained from the 300 run ensemble of SELECTOR results to perform an inversion for some synthetic line intensities. Here we perform a similar analysis for the lines, identified by Vernazza & Reeves (1978), observed by the Harvard S-055 Spectroheliometer (Reeves et al. 1977) on the Apollo Telescope Mount during the 1973–1974 *Skylab* mission. Once we have obtained this optimal subset of lines, we perform a series of inversions to infer the $\xi(t_e)$ of the emitting solar plasma.

We make use of the same atomic models described in § 2 but we concentrate on the 40 strong lines identified in the composite (average) quiet-Sun spectra of Vernazza & Reeves (1978; Figs. 2, 3, and 4) that occur in the instrument's 280–1350 Å wavelength range. To offset the reduction in the number of lines used in this study we are careful to include the emissivities from lines (particularly of the same ionic multiplets) that form blends with those lines identified within the spectral resolution of the instrument (1.6 Å FWHM), in addition to those blends noted in the tables of Vernazza & Reeves (1978). We then find that some 87 emissivities combine linearly to form the 40 used in the present analysis.

The reduction to an analysis of only 40 lines dramatically reduces the dimensionality of the search problem, even more so since we now proceed to select a further subset of $M = 30$ lines. There are now some 10^{11} possible combinations of line emissivities (calculated, in this case, for a constant electron pressure $P_e = n_e T_e = P_o = 4 \times 10^{14}$ cm^{-3} K, taken from Table 1 of RD1981b) that could form the "optimal" set (cf. $n \approx 10^{29}$ of § 2.4). The assumption of constant P_e is not only to make comparison with the calculations of RD1981b but to ensure that the calculations are consistent with observations and currently accepted models of the solar transition region (TR), which suggest that the TR is a constant pressure interface between the chromosphere and corona, see, e.g., chap. 6 of Mariska (1992). Again, we fix the number of t_e discretization points to $P = 30$, uniformly distributed in t_e over the range $4.0 \leq t_e \leq 6.5$.

The $N = 40$ "All-lines" case now has $\log_{10} C_K = 7.6727$. On the other hand, the optimal line set obtained by SELECTOR yields $\log_{10} C_K = 6.6091$, again an order of magnitude smaller. We tabulate these results in Table 4 by indicating the number of times that each line was selected,

[6] We have used the numbers from Fig. 3 of RD1981b and interpolated a best fitting curve to the points. This curve is then our "model" $\xi(t_e)$ and is used to compute synthetic line intensities for the 133 lines by calculating the result of eq. (8) for each. Such calculations are termed as "forward" calculations, using the right-hand side of eq. (8) to determine the left-hand side. The model curve of RD1981b is then the target function of the "backward," or inverse, process.

[7] The fact that we can obtain a physical solution by imposing significantly less regularization is another bonus of the SELECTOR preconditioning step.

TABLE 4

DETAILS OF THE 40 STRONG EMISSION LINES IN THE WAVELENGTH RANGE OF THE HARVARD S-055 SPECTROHELIOMETER (280–1350 Å) SELECTED AT THE END OF THE 300–3000 GENERATION RUNS OF SELECTOR

Ion	λ (Å)	Count	$t_e^{\max}$	Ion	λ (Å)	Count	$t_e^{\max}$
C II	903.962	255	4.338*	C II	1037.02	114	4.338*
C II	1335.66	264	4.338	C III	977.017	231	4.775*
C III	1175.71	198	4.775*	Mg VIII.....	430.465	255	5.896*
Mg VIII.....	436.670	255	5.896*	Mg IX	368.070	267	5.982*
Mg X	609.793	234	6.068*	Mg X	624.941	231	6.068
Ne VI.....	401.136	240	5.551*	Ne VI.....	558.594	165	5.551
Ne VI.....	562.701	180	5.551*	Ne VII	465.219	192	5.724
Ne VIII	770.409	240	5.724	Ne VIII	780.324	237	5.724*
Si II.....	1264.74	264	4.258*	Si III	1206.50	243	4.689*
Si XII	499.406	261	6.241*	Si XII	520.665	249	6.241*
N II.....	1085.53	276	4.517*	N III	685.817	261	4.948*
N III	989.799	138	4.862*	N III	991.511	171	4.862
N V.....	1238.82	231	5.206*	N V.....	1242.80	240	5.206*
O II.....	718.505	249	4.603*	O II.....	833.330	219	4.603*
O II.....	834.465	207	4.603	O III	525.797	243	4.948
O III	599.598	204	4.948*	O III	702.332	240	4.862*
O IV	553.329	231	5.206	O IV	787.710	252	5.120*
O IV	790.199	177	5.120	O V.....	629.730	66	5.379
O V.....	758.675	201	5.379*	O VI.....	1031.91	270	5.465*
Fe XV	284.160	297	6.327*	Fe XV	417.258	252	6.327*

NOTES.—The lines indicated by an asterisk (*) are those belonging to the set having the minimum value of $\log_{10} C_K = 6.6091$. Also given are the ions to which the line belongs, wavelengths λ (Å), the number of times the line was selected and the temperature ($t_e = \log_{10} T_e$) at with the emissivity of the line peaks, $t_e^{\max}$.

the temperature at which $K_l(t_e)$ peaks ($t_e^{\max}$) and if they belong to the optimal set (determined as above; identified by an asterisk).

Before considering formal inversions of the S-055 line intensities for the "All-lines" and SELECTOR line sets it is important to try and reproduce the quiet-Sun average $\xi(t_e)$ function in Figure 1 of Raymond & Doyle (1981a). We do this using their inversion technique but our line emissivities, since we benefit from improved determinations, in the intervening years, of many of the underlying atomic coefficients. The Raymond & Doyle method of inferring the $\xi(t_e)$ function explicitly assumes that $\xi(t_e)$ does not vary over regions smaller than $\Delta t_e = 0.1$ such that equation (8) becomes

$$I_l = \xi(t_l^*) \int_{t_e} K_l(t_e) dt_e \tag{22}$$

where t_l^* is the peak emissivity temperature of the line labeled l. The $\xi(t_e)$ function is then readily constructed by using the M lines, each giving a value $\xi(t_l^*)$ given by

$$\xi(t_l^*) = I_l^{\rm obs} \left[\int_{t_e} K_l(t_e) dt_e \right]^{-1} . \tag{23}$$

With the $\xi(t_e)$ function of RD1981b duplicated, noting that we have adjusted our elemental abundances (Grevesse & Anders 1991) to those given in Table 1 of Raymond & Doyle (1981a), we may proceed with a comparison between our formal regularized inversions and their results.

In Figure 10 we present the inversions for the observed line intensities of Vernazza & Reeves (1978). As for Figure 8 we have performed the inversion for a range of smoothing parameters ($10^1 \le \Lambda \le 10^4$ in this case) for the SELECTOR optimal set (*solid line*) and the "All-lines" set (*dot-dashed line*). These are plotted, for comparison, against the average quiet-Sun $\xi(t_e)$ (RD1981b) (*dashed line*). We see from Figures 10*a*–10*d* that both the "All-lines" and SELECTOR set inversions recover the trend of the RD1981b $\xi(t_e)$ behavior for $5.0 \le t_e \le 6.5$. Also note that both inversions, for low Λ, reproduce the maximum at $t_e \approx 6.2$, but given the discussion of the previous section and probable error amplification present, can it be taken from granted that this feature is physical, as opposed to an inversion artifact ?

Figures 11*a* and 11*b* show two "All-lines" inversions, obtained with $\Lambda = 10$ (*a*) and $\Lambda = 1$ (*b*), with error bars (as calculated in § 3) now included. Figure 11*c* shows a SELECTOR-preconditioned solution with $\Lambda = 10$. Notice how the error estimates in this case are much smaller than the equivalent "All-lines" solution of Figure 11*a*. To bring the error bars of the "All-line" solution down to comparable levels requires a decrease of the regularization to $\Lambda = 1$ (Fig. 11*b*), but the solution is then clearly numerically unstable.

A very powerful way to carry out the solution of an ill-conditioned matrix system is based on singular value decomposition (SVD; see Press et al. 1992, § 2.6); the technique consists in forming as many orthogonal (or near-orthogonal) linear combinations of the kernel emissivities as possible, given the original emissivity kernal matrix. If the problem is indeed ill conditioned, there will be fewer such linear combinations than original emissivities, which will lead to very small singular values for some linear combinations. The heart of the SVD-based technique is to eliminate these deleterious combinations by zeroing the corresponding inverse singular values in the singular value matrix (see Press et al. 1992, *ibid.*). The dash-dotted line on Figure 11*c* is a solution obtained in this way, with an inverse singular value threshold of 10^{-2} (meaning that 26 of

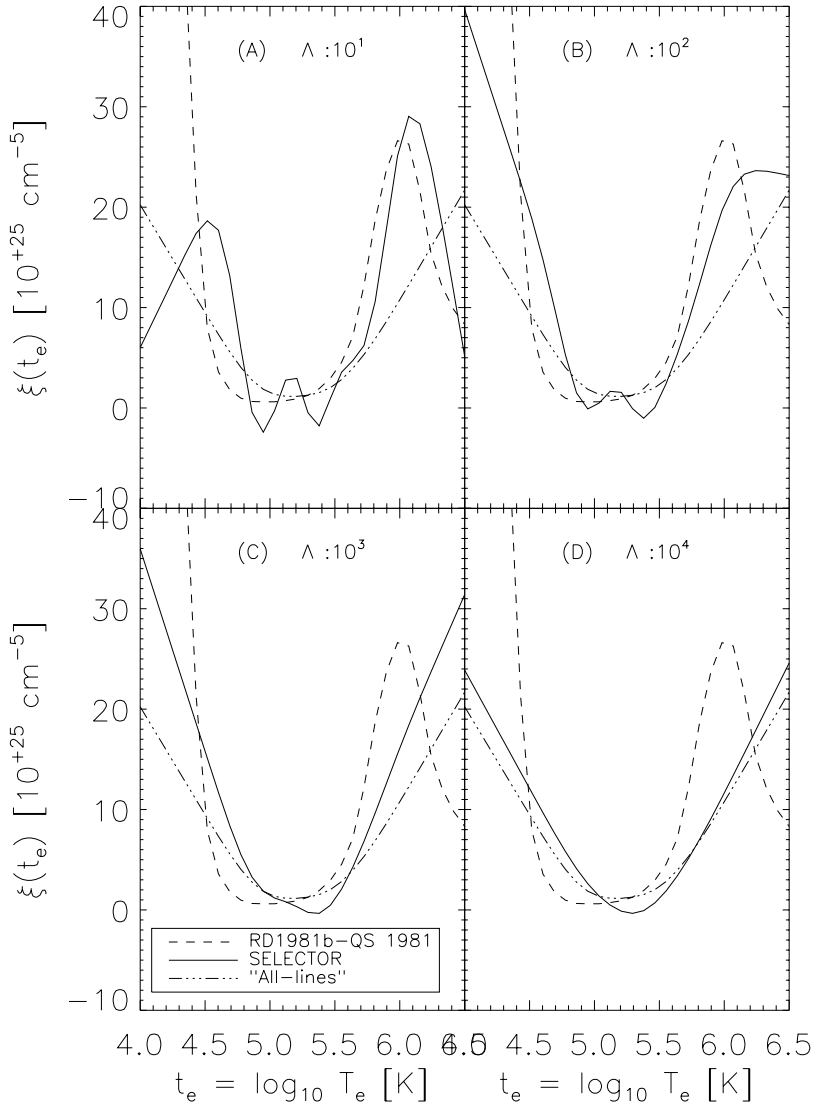

FIG. 10.— Tichonov regularized inversion (for smoothing parameters, Λ, varying from 10^1 to 10^4) of the average quiet-Sun line intensities taken from Vernazza & Reeves (1978) and identified in Table 4. The SELECTOR $\xi(t_e)$ function recovered (*solid line*) is more numerically stable than that for the "All-lines" (*dot-dashed line*) approach in the presence of errors in the line intensities. Against these functions we plot the DEM curve published by Raymond & Doyle (1981b) for the same data (*dashed line*; labeled as RD1981b-QS). As for Fig. 8 we see that the SELECTOR solution is physical for a lower value of Λ (only 1 order of magnitude in this case).

40 linear combinations are retained for the inversion). The SVD solution is quite similar to the SELECTOR-preconditioned regularized solution, indicating that both methods succeed about equally well in mitigating the ill-conditioned nature of the Kernel emissivity matrix.

Both $\Lambda = 10$ solutions on Figure 11 show a statistically significant peak at $t_e \simeq 6$. At lower temperatures, specifically around $t_e \leq 4.5$, the preconditioned solution shows a downturn relative to the RD1981b curve. However, the $\xi(t_e)$ inferred by these authors is determined by a single C II line at 1335 Å (see Table 2 of Raymond & Doyle 1981a) and so may not be properly constrained by the data. Examination of Table 4 will reveal that our inversion includes information from four lines in the "All-lines" set, and three in the optimal set. However, we note also that the optimal inversion does not determine the intensity of the Si II 1265 Å line either which suggests that $\xi(t_e)$ *must* rise by a factor of around 4 in that region. The erroneously low intensities for these two (relatively strong) lines indicates that the observational errors may have been underestimated and were thus not given enough weight in the inversion.

In Table 5 we list the observed intensities of Vernazza & Reeves (1978) along with a forward calculation using the RD1981b $\xi(t_e)$ and the form of $\xi(t_e)$ we infer using the "All-lines" second-order regularization ($\Lambda = 10^3$; i.e., from Figure 10*c* where the solution is positive-definite). It is clear that there is reasonable correspondence between the inferred intensities from the two methods and the observed intensities, except for some of the ionic lines formed at $t_e \leq 4.4$.

A detailed investigation of the low-t_e discrepancy in the $\xi(t_e)$ functions is beyond the scope of this paper, although a reevaluation of the observational errors may be enough to produce a result better fitted to the data at low t_e. We simply point out that the few lines available in this t_e range imply that regularization will strongly influence, perhaps even dominate, the behavior of the solution. The choice of regularization technique, in this case, then becomes critical.

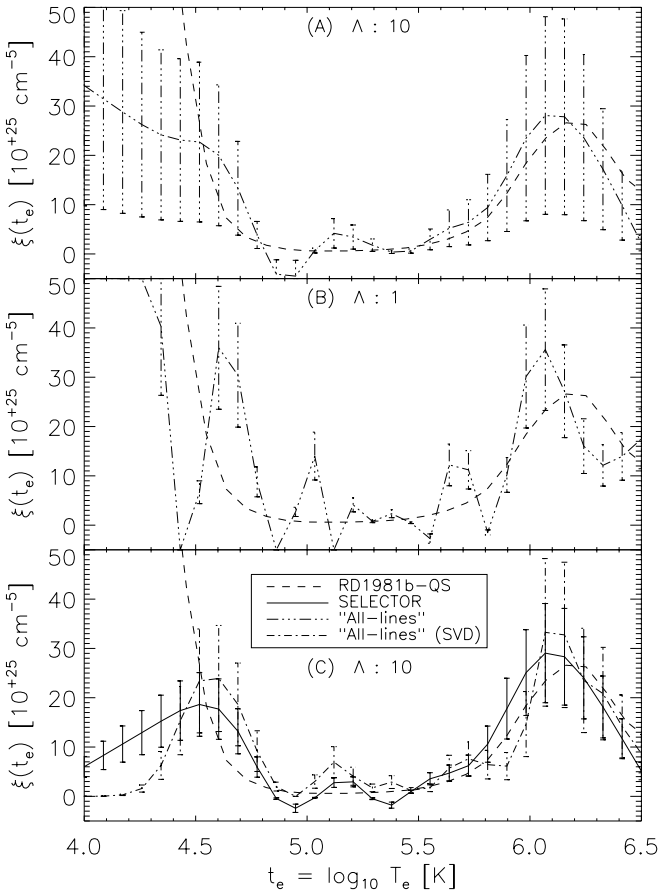

FIG. 11.—Tichonov regularized inversions for the quiet-Sun average spectrum of Vernazza & Reeves (1978) with a comparable magnitude in their error bars. Shown are the inversions for the "All-line" case with $\Lambda = 10$ (*a*) and $\Lambda = 1$ (*b*), and for the SELECTOR optimal line set (*b*), also with $\Lambda = 10.0$. The DEM curve published by Raymond & Doyle (1981b) for the same data is plotted as a dashed line on all panels. Comparing (*a*) and (*c*), Notice again the smaller error bars associated with the SELECTOR preconditioned solution, for a fixed value of Λ. Reducing the "All-lines" error bars to comparable magnitude requires a decrease of Λ to the level where the solution is numerically unstable (*b*). Again, the positivity issues in these solutions are clear (cf. Fig. 8).

It would certainly be useful to use a nondifferential smoothing regularization, such as is provided by a maximum entropy formulation (see, e.g., Press et al. 1992, § 18.7).

5. DISCUSSION

In this paper we have aimed at improving the accuracy and reliability of DEM analysis of emission lines. We have described a form of preconditioning step to the DEM inversion proper, which consists in selecting a *subset* of spectral lines to be used for the inversion, rather than using all the physically suitable lines available in the data set under investigation. Working on the sets of UV/EUV lines available in the *SOHO* SUMER/CDS and Harvard S-055 EUV Spectroheliometer data sets, we have achieved reduction by a factor of 10 in the condition number of the discretized integral operator. The associated improvement in numerical stability allows us to compute inversions with significantly smaller regularization. This, in turn, leads to DEM determinations that are formally more accurate, and more physically meaningful.

There is another, purely practical advantage to carrying out this kind of preconditioning. The number of emission lines used to perform the DEM inversion can be reduced, sometimes drastically (cf., going from 133 to 30 lines in the case of *SOHO* SUMER/CDS data). The size of the corresponding inverse problem is reduced proportionally, which can translate to large reduction in needed CPU time (inversion is typically a N^3 operation, for a square problem, where N is the size of the matrix representation of the integral operator). The speedup incurred by making use of the preconditioning step advocated in this paper can obviously facilitate the analysis, in a reasonable amount of CPU time, of very large spectral data set (e.g., sequences of high spatial resolution spectra obtained at a high time cadence), without compromising the accuracy of the numerical inversions.

In a forthcoming paper (McIntosh & Charbonneau 2000) we will expand on the present analysis by considering simple extensions. Given the flexibility of our genetic algorithm-based combinatorial optimization scheme, it is a simple matter to let the number of emission lines considered in the calculation be itself a quantity being varied toward optimization. Likewise, the use of singular value decomposition to compute the condition number, although more computationally demanding than the approximate technique of Clive et al. (1979), would allow one to consider situations where the number of discretization point P is either larger or smaller than the number of emission lines being used for the analysis. Another matter to be address there is the incorporation of an "observability factor" for each line into SELECTOR. This will address the practicality of making the actual observation, i.e., a preconditioning step for making UV/EUV observations of particular lines with regard to performing reliable DEM(T_e) functions, and not on lines already observed (as we have done here), and is hence omitted from this paper.

The possibility to easily incorporate observational and/or physical constraints to the line selection process is a notable advantage of our approach, which does not readily carry over to classical approaches to condition number mitigation, such as inversions based on singular value decomposition. In fact our SELECTOR technique represents a form of "zeroth-order" SVD, in which emissivities are either retained or tossed away. The price to pay is that we are throwing away information that could be put to good use by SVD; the advantage lies with flexibility in incorporating constraints in the line selection process. The results reported in this paper indicate that our advocated preconditioning step, though in principle inferior to formal SVD in its use of whatever information is present in the data, still leads to numerical inversions that are similar to those obtained via SVD, in that both are numerically much better behaved than a direct inversion of the "All-lines" Kernel.

On the physical front, it will be interesting to examine whether our preconditioning scheme can improve the notoriously difficult inversion for the differential emission measure in n_e (see Almleaky, Brown, & Sweet 1989). The extremely poor conditioning of the DEM(n_e) inverse problem is caused by the functional behavior of the line emissivities as a function of n_e; see, e.g., Dere & Mason 1981; Mason & Monsignori-Fossi 1994). Likewise, it will be interesting to apply a preconditioning step to improve the stability and accuracy of the bivariate DEM inverse problem discussed in Judge et al. 1997 (see eq. [3]).

To sum up, we have shown, in the context of the DEM(T_e) inverse problem, that judicious selection of a

TABLE 5

INTENSITIES OF THE 40 STRONG EMISSION LINES FOR THE QUIET-SUN AVERAGE SPECTRUM TAKEN FROM VERNAZZA & REEVES 1978 (I_{obs})

Ion	λ (Å)	I_{obs}	I_{RD}	I_{MCB}	Ion	λ (Å)	I_{obs}	I_{RD}	I_{MCB}
C II	903.962	32.89	213.93	55.31	C II	1037.02	204.30	259.70	290.58
C II	1335.66	1205.02	1129.09	252.10	C III	977.017	963.06	2020.92	773.00
C III	1175.71	314.80	714.48	282.79	Mg VIII.....	430.465	38.22	10.66	28.05
Mg VIII.....	436.670	42.70	15.09	39.33	Mg IX	368.070	655.00	72.62	160.06
Mg X	609.793	125.05	53.75	83.23	Mg X	624.941	51.43	26.61	41.25
Ne VI.....	401.136	89.00	13.85	35.01	Ne VI.....	558.594	18.95	4.19	10.60
Ne VI.....	562.701	18.31	7.51	18.76	Ne VII	465.219	120.32	20.86	60.62
Ne VIII	770.409	53.75	24.77	56.73	Ne VIII	780.324	25.93	12.39	28.44
Si II.....	1264.74	148.85	27.05	5.10	Si III	1206.50	694.59	804.35	238.01
Si XII	499.406	51.35	70.18	78.66	Si XII	520.665	25.44	33.81	37.90
N II.....	1085.53	72.74	98.89	26.03	N III	685.817	23.71	75.47	34.89
N III	989.799	34.73	51.69	22.12	N III	991.511	47.22	103.75	44.46
N V.....	1238.82	61.37	27.13	58.98	N V.....	1242.80	36.46	15.65	32.32
O II.....	718.505	14.56	17.91	5.32	O II.....	833.330	73.23	155.14	61.31
O II.....	834.465	23.24	255.04	101.89	O III	525.797	31.20	15.56	7.90
O III	599.598	56.59	43.70	21.38	O III	702.332	75.29	63.18	29.34
O IV	553.329	44.39	16.52	27.11	O IV	787.710	83.15	52.98	73.57
O IV	790.199	159.45	105.19	145.21	O V.....	629.730	334.97	161.25	374.23
O V.....	758.675	7.68	3.13	7.31	O VI	1031.91	305.28	155.71	294.00
Fe XV[a]	284.160	0.00	...	...	Fe XV	417.258	33.73	17.56	18.92

NOTES.—Intensities of the 40 strong emission lines for the quiet-Sun average spectrum taken from Vernazza & Reeves 1978 (I_{obs}). Also given are the intensities calculated (via eq. [8]) for the Raymond & Doyle 1981b (I_{RD}) and second-order regularization (I_{MCB}; for $\Lambda = 10^3$) $\xi(t_e)$ functions.

[a] The line of Fe XV at 284.160 Å is omitted from the inversions since it has zero intensity in Vernazza & Reeves 1978.

subset of emission lines leads to inversions of the source function that exhibit better accuracy and numerical stability than if all available lines are used. At first glance this is a very counterintuitive result; how can one obtain a superior solution by making use of *less* information? The answer, of course, is that the information being discarded is in fact redundant, and moreover dangerously so from a numerical point of view.

The authors would like to thank Phil Judge and Hanli Liu for their help and for some interesting discussions during the completion of this work. In addition, we would like to thank Carole Jordan for a thorough reading and for raising many interesting points during the refereeing process. S. Mc. acknowledges the support of a UK PPARC studentship during which this research was carried out. Both S. Mc. and J. C. B. are grateful for the support of the HAO visitor program.

REFERENCES

Almleaky, Y. M., Brown, J. C., & Sweet, P. A. 1989, A&A, 224, 328
Arnaud, M., & Rothenflug, R. 1985, A&AS, 60, 425
Brown, J. C., Dwivedi, B. N., Sweet, P. A., & Almleaky, Y. M. 1991, A&A, 249, 277
Charbonneau, P. 1995, ApJS, 101, 309
Charbonneau, P., & Knapp, B. 1996, A User's Guide to PIKAIA 1.0: (NCAR Techn. Note 418 + IA)
Clive, A. K., Moler, C. B., Stewart, G. W., & Wilkinson, J. H. 1979, SIAM J. Numer. Anal., 16, 368
Craig, I. J. D., & Brown, J. C. 1976, A&A, 49, 239
———. 1986, Inverse Problems in Astronomy: A Guide to Inversion Strategies of Remotely Sensed Data (Bristol: Adam Hilger)
Dere, K., & Mason, H. E. 1981, in Solar Active Regions, ed. F. Q. Orall (Boulder: Colorado Associated Univ.), 129
Doschek, G. A. 1987, in Theoretical Problems in High Resolution Solar Physics II, ed. R. G. Athay & D. S. Spicer (NASA CP-2483), 37
Doyle, J. G., Raymond, J. C., Noyes, R. W., & Kingston, A. E. 1985, ApJ, 297, 816
Fleck, B., Domingo, V., & Poland, A. I. 1995, The *SOHO* Mission (Dordrecht: Kluwer)
Goldberg, D. A. 1989, Genetic Algorithms in Search of Optimization and Machine Learning (New York: Addison Wesley)
Golub, G. H., & Van Loan, C. F. 1989, Matrix Computations (2d ed.; Baltimore: Johns Hopkins Univ. Press)
Grevesse, N., & Anders, E. 1991, in Appendix A: Solar Element Abundances, in Solar Interior and Atmosphere, ed. A. N. Cox, W. C. Livingstone, & M. S. Matthews (Tucson: Univ. Arizona), 1227
Harrison, R. A., et al. 1995, Sol. Phys., 162, 233
Holland, J. H. 1962, J. Assoc. Comp. Mach., 3, 297
Jacobs, V. L., Davis, J., Kepple, P. C., & Blaha, M. 1977, ApJ, 211, 605
Jacobs, V. L., Davis, J., Robertson, J. E., Blaha, M., Cain, J., & Davis, M. 1980, ApJ, 239, 1119
Jefferies, J. T., Orrall, F. Q., & Zirker, J. B. 1972a, Sol. Phys., 22, 307
———. 1972b, Sol. Phys., 22, 317
Jin, Q., & Hou, Z. 1997, Inverse Problems, 13, 815
Jordan, C. 1969, MNRAS, 142, 501
Jordan, C., & Wilson, R. 1971, in NATO Advanced Study Institute, Physics of The Solar Corona, ed. C. J. Macris (Dordrecht: Reidel), 219
Judge, P. G., Hubeny, V., & Brown, J. C. 1997, ApJ, 475, 275
Judge, P. G., & Meisner, R. 1994, in The Third *SOHO* Workshop, Solar Dynamic Phenomena and Solar Wind Consequences, ed. J. J. Hunt (ESA SP-373), 67
Judge, P. G., Woods, T. N., Brekke, P., & Rottman, G. J. 1995, ApJ, 455, L85
Kashyap, V., & Drake, J. J. 1998, ApJ, 503, 450
Lanzafame, A. C., Brooks, D. H., Summers, H. P., Thomas, R. J., & Thompson, A. M. 2000, preprint
Louis, A. K. 1996, Inverse Problems, 12, 175
Mariska, J. T. 1992, The Solar Transition Region (Cambridge: Cambridge Univ. Press)
Mason, H. E., & Monsignori-Fossi, B. C. 1994, A&A Rev., 6, 123
McIntosh, S. W. 1998, Ph.D. thesis, Univ. Glasgow
McIntosh, S. W., Brown, J. C., & Judge, P. G. 1998a, A&A, 333, 333
McIntosh, S. W., & Charbonneau, P. 2000, in preparation
Michalewicz, Z. 1994, Genetic Algorithms + Data Structures = Evolution Programs (New York: Springer)
Mitchell, M. 1996, An Introduction to Gentic Algorithms (Cambridge: MIT)

Munro, R. H., Dupree, A. K., & Withbroe, G. L. 1971, Sol. Phys., 19, 347
Noyes, R. W., Raymond, J. C., Doyle, J. G., & Kingston, A. E. 1985, ApJ, 297, 805
Parker, R. L. 1994, Geophysical Inverse Theory (Princeton: Princeton Univ. Press)
Pottasch, S. R. 1964, Space Sci. Rev., 3, 816
Press, W. H., Teukolsky, S. A., Vetterling, W. T., & Flannery, B. P. 1992, Numerical Recipes in Fortran (2d ed.; Cambridge: Cambridge Univ. Press)
Raymond, J. C., & Doyle, J. G. 1981a, ApJ, 245, 1141
———. 1981b, ApJ, 247, 686 (RD1981b)
Reeves, E. M., Huber, M. C., & Timothy, J. G. 1977, Appl. Opt., 16, 837
Sneddon, I. N. 1972, The Use of Integral Transforms (New York: McGraw-Hill)
Thompson, A. M. 1991, in Integral Intensity Inversion Techniques: A Study in Preparation for the *SOHO* Mission Rutherford Appleton Laboratory, ed. A. M. Thompson & R. A. Harrison (RAL91-092)
Tichonov, A. N. 1963, Soviet Maths Dokl., 4, 1035
Twomey, S. 1963, J. Ass. Comp. Mach., 10, 97
Vernazza, J. E., & Reeves, E. M. 1978, ApJS, 37, 485
Wilhelm, K., et al. 1995, Sol. Phys., 162, 189
Withbroe, G. L. 1970, Sol. Phys., 11, 41
———. 1975, Sol. Phys., 45, 301